Supporting Information

Deciphering the interaction mechanism between copper and polysulfides for enhanced performance and cost-efficiency in quasi-sodium-sulfur batteries

Haobin Song[1,#], Tong Li[1,#], Tingting He[1], Guanghui Chen[1], Chengjiang Deng[1], Dezhi Kong[2], Dong Yan[3], Hui Ying Yang[4,*], Shaozhuan Huang[1,*]

[1]Key Laboratory of Catalysis and Energy Materials Chemistry of Ministry of Education & Hubei Key Laboratory of Catalysis and Materials Science, South-Central Minzu University, Wuhan 430074, Hubei, China.

[2]Key Laboratory of Material Physics, Ministry of Education, School of Physics and Microelectronics, Zhengzhou University, Zhengzhou 450052, Henan, China.

[3]International Joint Laboratory of New Energy Materials and Devices of Henan Province, School of Physics & Electronics, Henan University, Kaifeng 475004, Henan, China.

[4]Pillar of Engineering Product Development, Singapore University of Technology and Design, 8 Somapah Road, Singapore 487372, Singapore.

[#]Authors contributed equally.

***Correspondence to:** Shaozhuan Huang, Key Laboratory of Catalysis and Energy Materials Chemistry of Ministry of Education & Hubei Key Laboratory of Catalysis and Materials Science, South-Central Minzu University, Wuhan 430074, Hubei, China. E-mail: husz001@scuec.edu.cn; Hui Ying Yang, Pillar of Engineering Product Development, Singapore University of Technology and Design, 8 Somapah Road, Singapore 487372, Singapore, E-mail: yanghuiying@sutd.edu.sg

Preparation of Na_2S_4 solution[1]**:** Sulfur powder, Na_2S, and NaOH (in a molar ratio of 3:1:1) were mixed in DI-water with continuous stirring for 12 h. The orange solution was acquired. 5 × 1 cm^2 metal strips of Cu and Al were soaked in 5 mL of 1 M Na_2S_4 aqueous solution for 10 mins and then taken out for characterization.

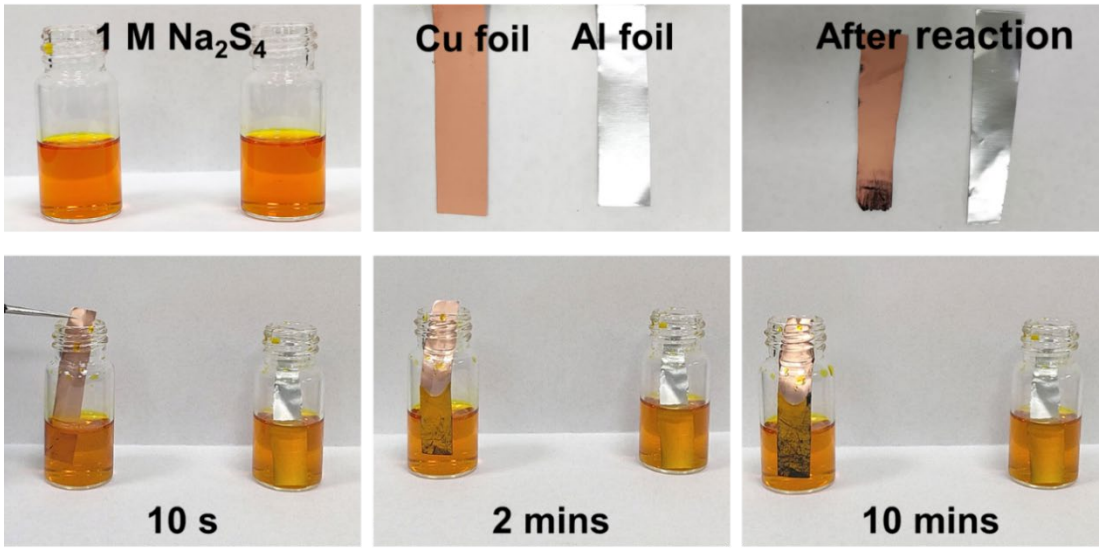

Figure S1. The optical picture of Cu foil and Al foil soaking in Na_2S_4 solution at different times. As revealed, the surface of the Cu foil becomes black after soaking for 10 mins, indicating the chemical reaction between Cu and Na_2S_4. While the Al foil remains unchanged, suggesting its chemical inertia toward Na_2S_4.

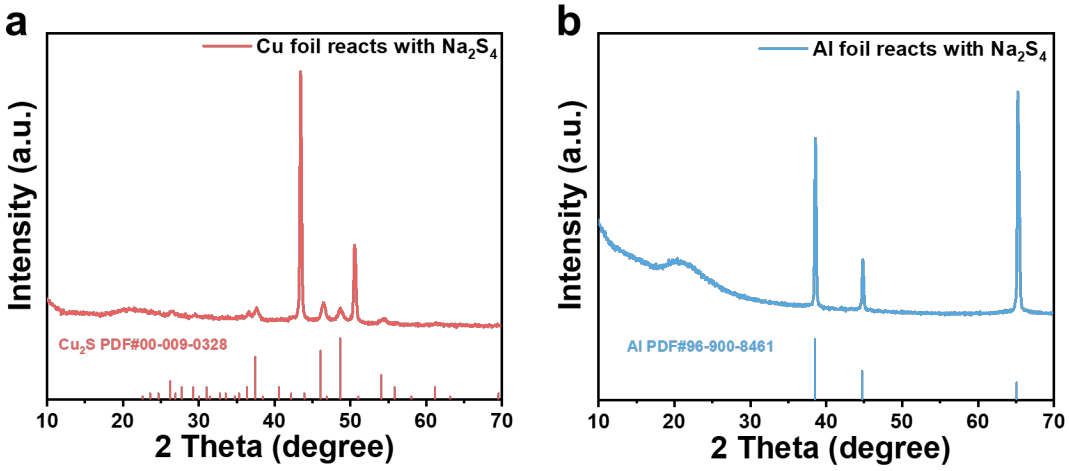

Figure S2. XRD pattern of Cu foil (a) and Al foil (b) after soaking in Na_2S_4 solution for 10 mins. The Cu foil shows obvious peaks from Cu_2S (PDF No. 00-009-0328),

confirming the chemical reaction between Cu and Na_2S_4.

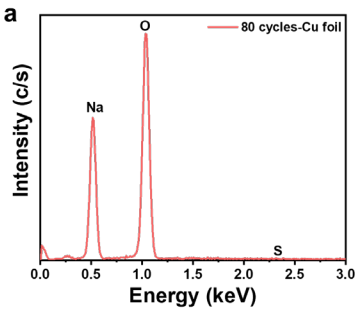

Elt.	Line	Intensity (c/s)	Atomic %	Conc	Units	
O	Ka	1,436.97	57.053	47.837	wt.%	
Na	Ka	2,248.69	42.065	50.680	wt.%	
S	Ka	82.44	.882	1.483	wt.%	
			100.000	100.000	wt.%	Total

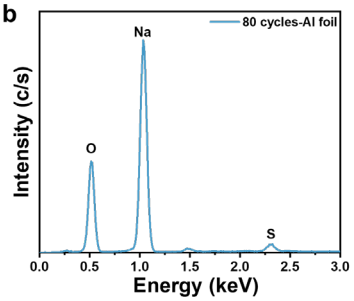

Elt.	Line	Intensity (c/s)	Atomic %	Conc	Units	
O	Ka	1,193.23	48.978	39.681	wt.%	
Na	Ka	3,086.89	49.014	57.059	wt.%	
S	Ka	198.87	2.008	3.260	wt.%	
			100.000	100.000	wt.%	Total

Figure S3. EDS (Energy Dispersive Spectrometer) of sodium metal after 80 cycles: (a). in CNT/S-Cu foil and; (b). CNT/S-Al foil. As shown in Figure S3, the sulfur signal from the cycled Na anode in DME-Al system is as high as 2%, much higher than that in the DME-Cu system.

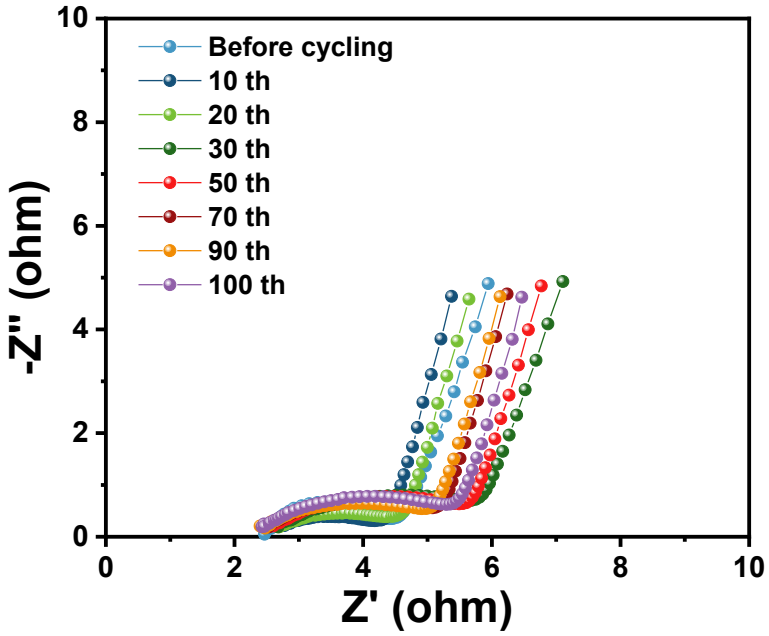

Figure S4. EIS spectra of CNT/S electrode at different cycles.

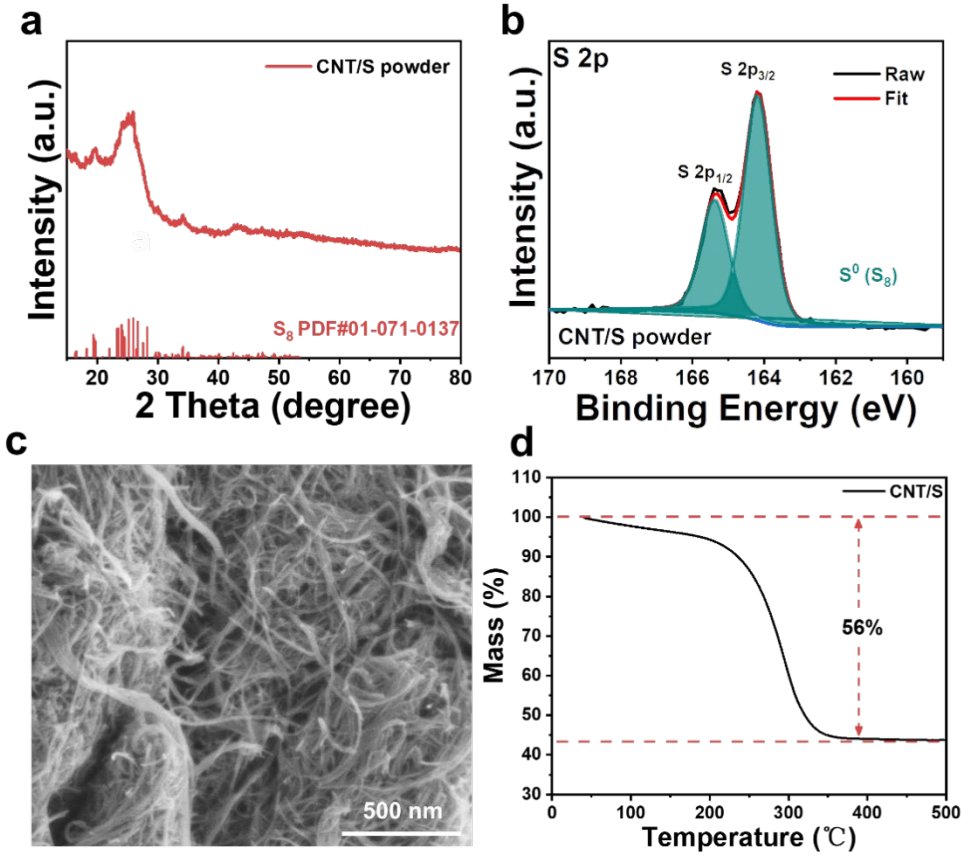

Figure S5. XRD pattern (a), S 2p XPS (b), SEM image (c) of the CNT/S powder and TGA of the CNT/S powder (d).

As shown in the X-ray diffraction (XRD) pattern [Figure S5a], the CNT/S powder shows very weak peaks corresponding to monoclinic S_8 (JCPDS No. 01-071-0137)[2]. S 2p X-ray photoelectron spectra (XPS) of the CNT/S powder exhibit two doublet peaks at 164.2 and 165.4 eV, corresponding to the S $2p_{3/2}$ and S $2p_{1/2}$ of S^0 [Figure S5b]. Scanning electron microscopy (SEM) image shows that the CNT/S powder mainly consists of nanotube morphology [Figure S5c], confirming the successful dispersion of sulfur in the CNT network. Besides, in Figure S5d, the TGA shows a sulfur loading of 56%.

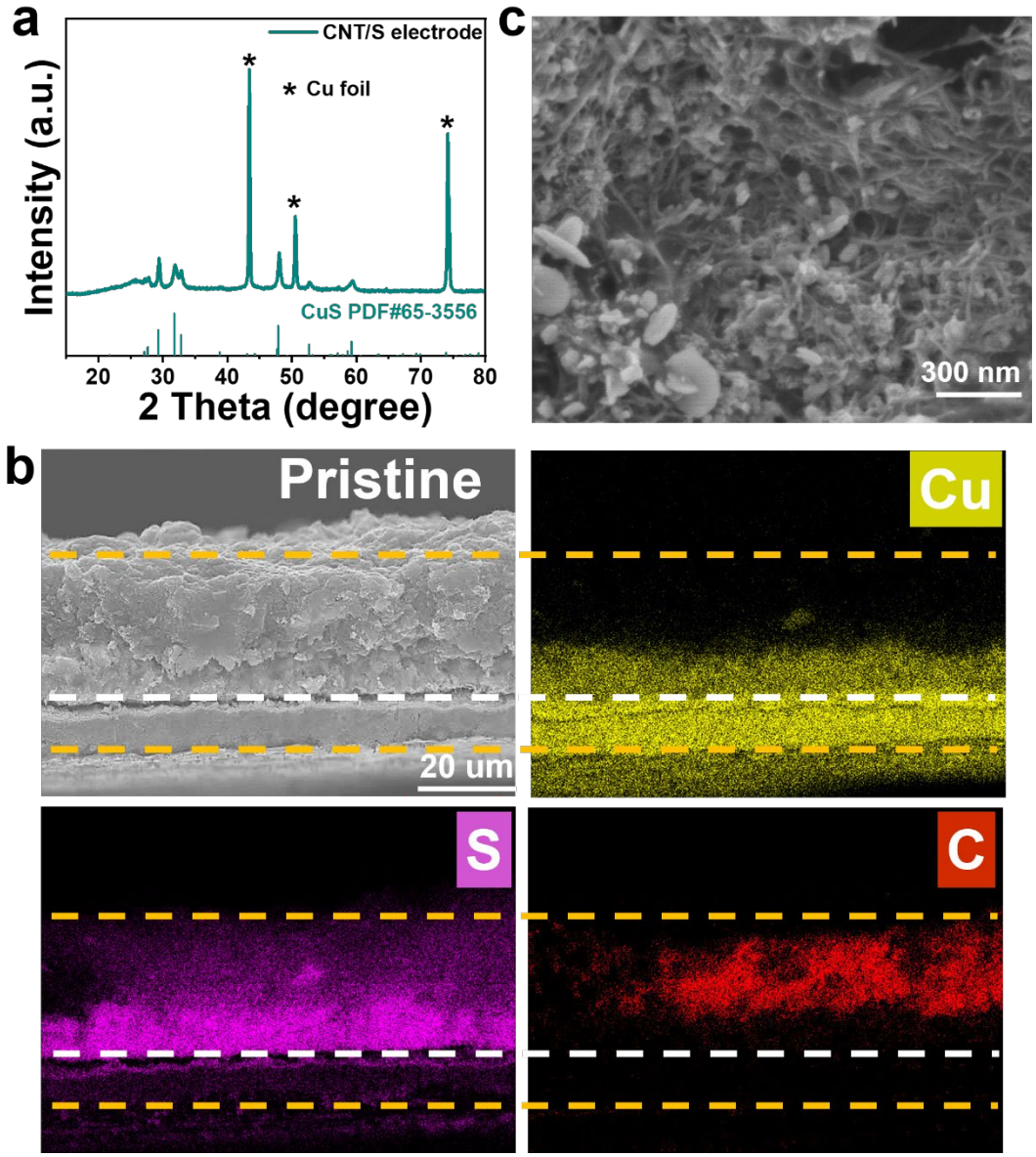

Figure S6. XRD pattern (a), SEM-EDX element mapping images (b), and SEM image (c) of CNT/S electrode.

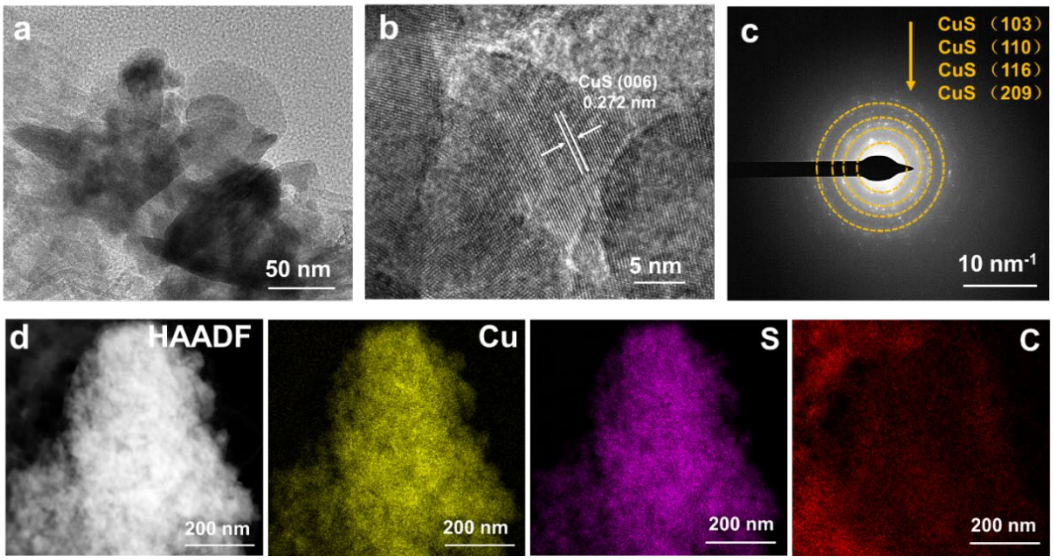

Figure S7. TEM (a) and HRTEM (b) images of CuS, (c) SAED pattern of CuS, (d) TEM-EDS mapping images of CuS.

TEM image reveals that the CuS shows an average size of around 50 nm [Figure S7a]. HRTEM image of CuS shows clear lattice fringes with interplanar spacing of 0.272 nm, corresponding to the (006) plane of hexagonal CuS [Figure S7b]. The corresponding SAED pattern shows a series of concentric rings [Figure S7c], which well match the standard patterns of cubic CuS. The STEM-EDS elemental mapping images of the CuS-S/CNT further confirm the uniform distribution of Cu and S elements [Figure S7d].

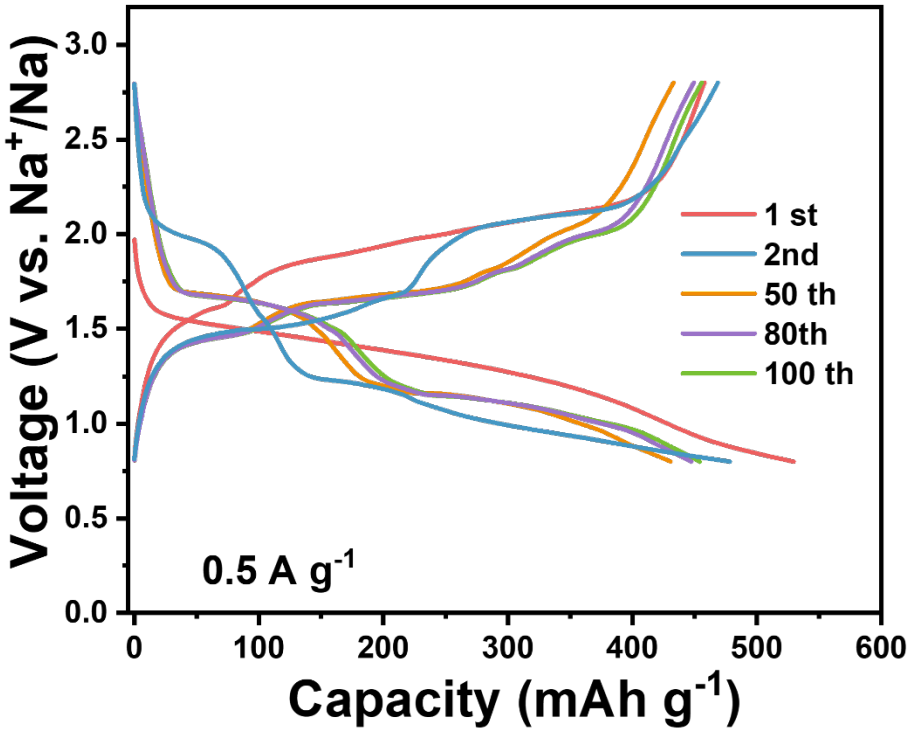

Figure S8. The charge-discharge curves of CNT/S at different cycles.

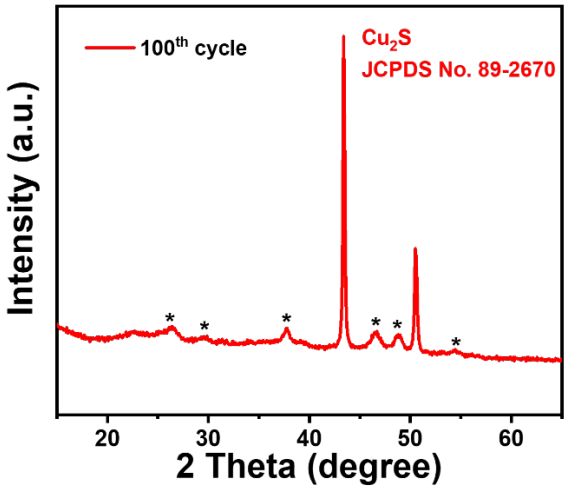

Figure S9. XRD patterns of CNT/S electrode after 100 cycles.

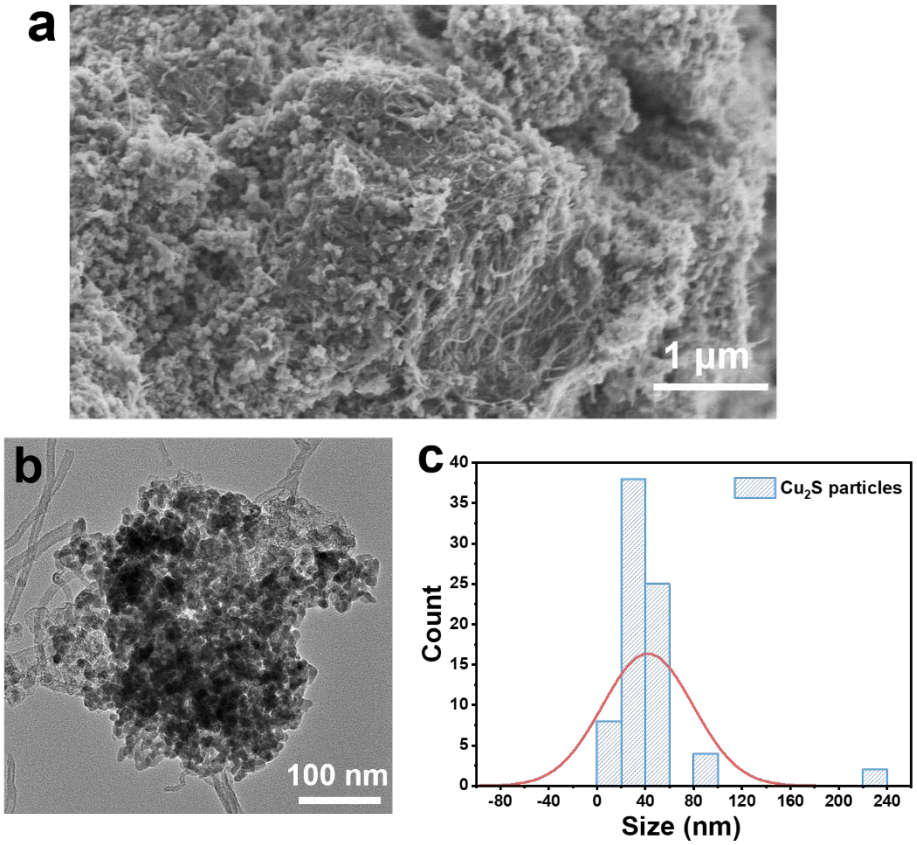

Figure S10. SEM (a), TEM image (b), and normal distribution of particle size for Cu_2S (c).

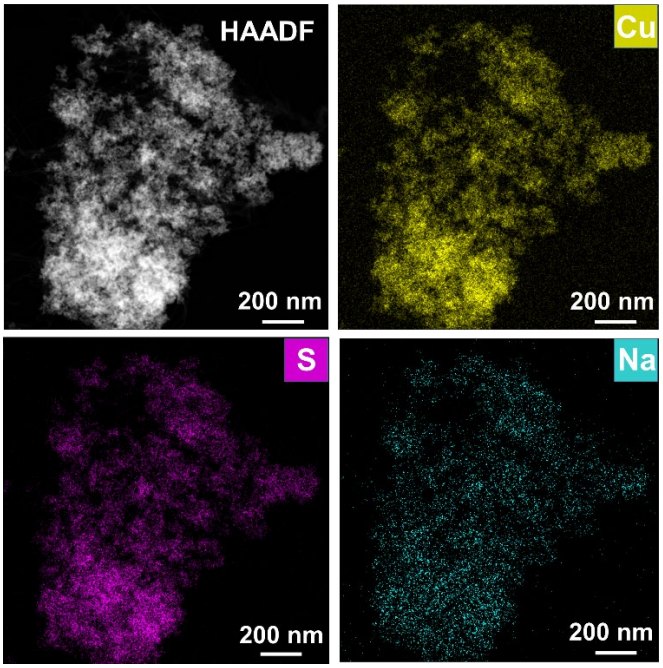

Figure S11. EDS elemental maps of CNT/S after 80 cycles.

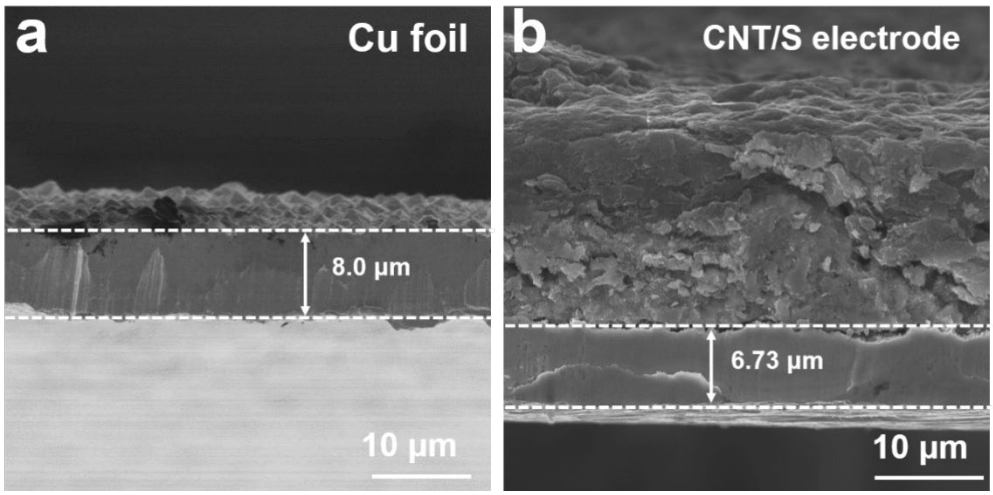

Figure S12. Cross-section SEM images of Cu foil (a) and CNT/S electrode (b). The pristine Cu foil shows a thickness of around 8 μm. We also calculated the thickness of the Cu foil through the mass of the Cu round pieces (diameter ~1.2 cm). The mass of ten pieces of Cu foil is around 81.5 mg, and the average mass of Cu foil is 8.15 mg. Then the thickness of Cu foil is calculated to be 8 μm based on the area and density of Cu foil.

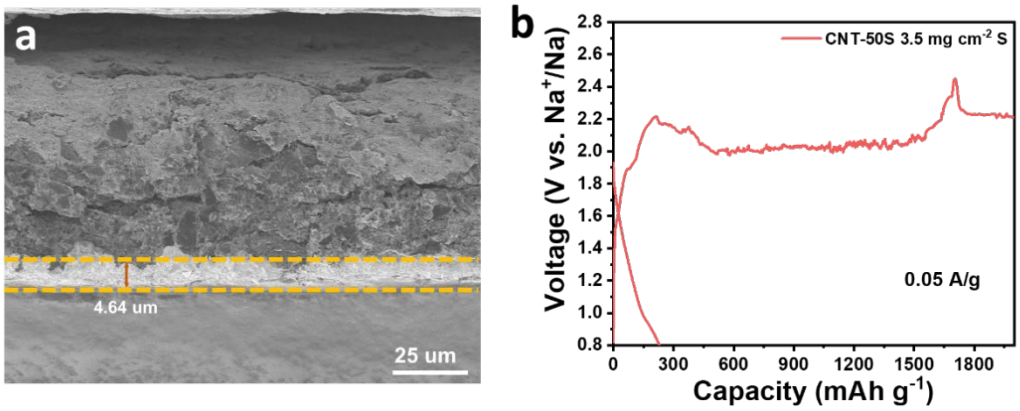

Figure S13. CNT/S electrode with a sulfur loading of 3.5 mg cm^{-2}: (a) cross-sectional SEM image of CNT/S electrode, and (b) charge-discharge curves.

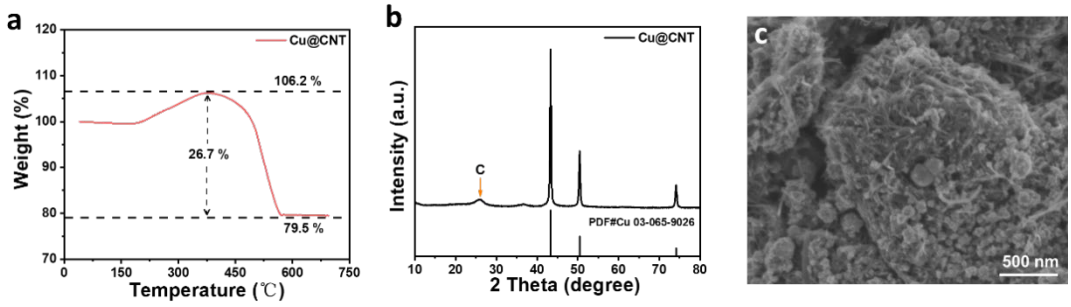

Figure S14. (a) Thermogravimetric analysis (TGA) of Cu@CNT in air. Cu@CNT was calcined in air to form CuO@CNT (106.2%), which was heated to 700℃, CNT (26.7% in CuO@CNT) transferred to CO_2 dispersed to air. After calculation, in Cu@CNT, the mass percentage of CNT is 36.5%. (b) XRD pattern of Cu@CNT powder, (c) SEM image of Cu@CNT powder.

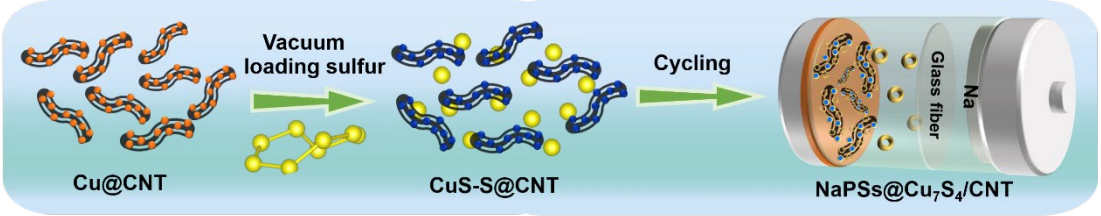

Figure S15. Schematic illustration of preparation and evolution of Cu@CNT/S.

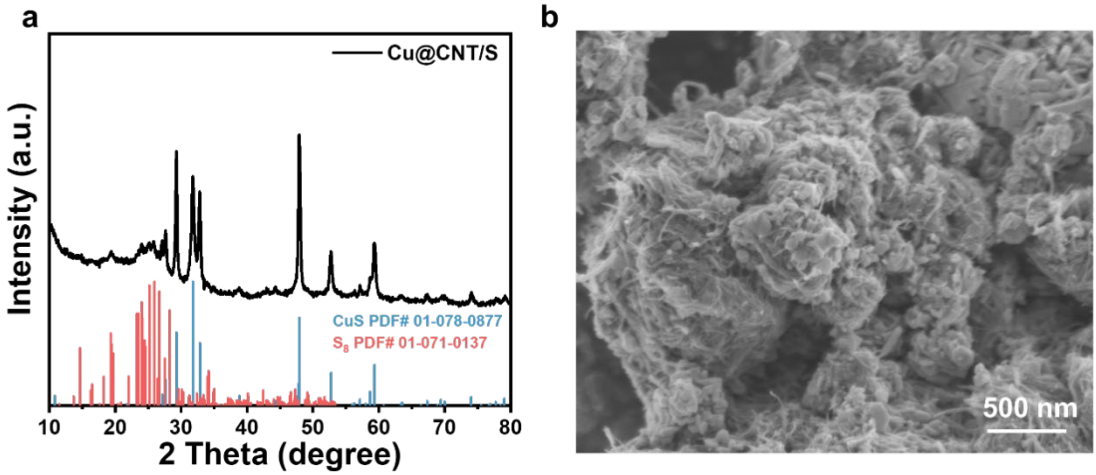

Figure S16. (a) XRD pattern of Cu@CNT/S, (b) SEM image of Cu@CNT/S powder.

As shown in Figure S16a, the XRD pattern includes S_8 (JCPDS No. 01-071-0137) and CuS (JCPDS No. 01-078-0877) crystalline phases, and in Figure S16b, the SEM

image shows nanotube CNT, particle S, and CuS.

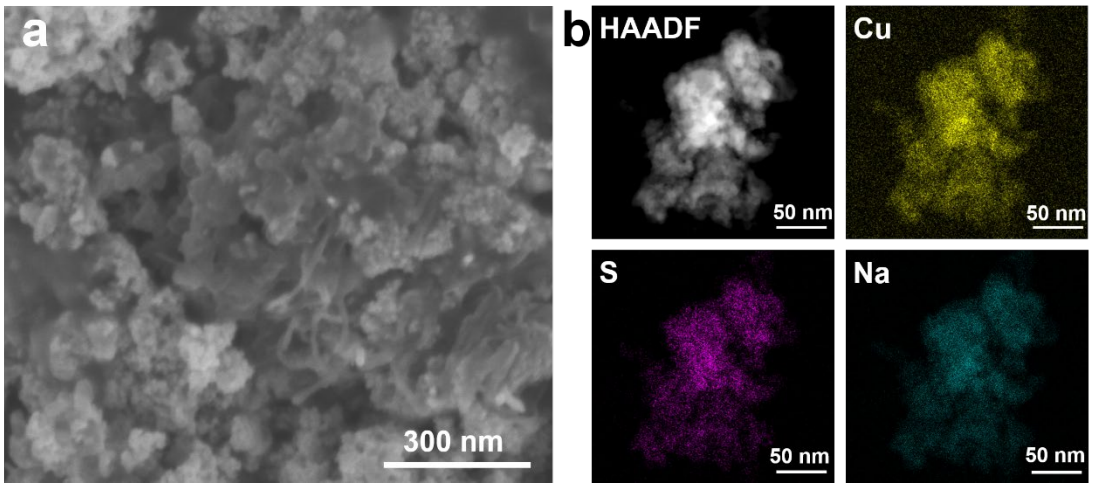

Figure S17. (a) SEM image of the Cu@CNT/S-80th, (b) STEM-EDX elemental maps of the Cu@CNT/S-80th.

SEM shows the Cu_7S_4 nanoparticles morphology which were dispersed into CNT network uniformly. Besides, STEM-EDX elemental mapping images indicate the Cu_7S_4 and NaPSs uniformly dispersed on the CNT surface.

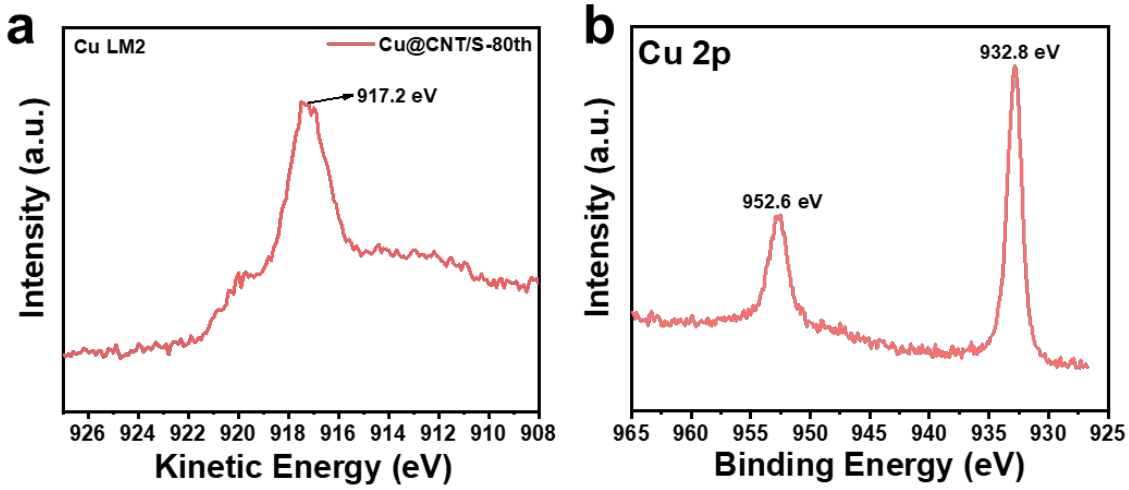

Figure S18. (a) AES and (b) XPS of Cu in Cu@CNT/S-80th.

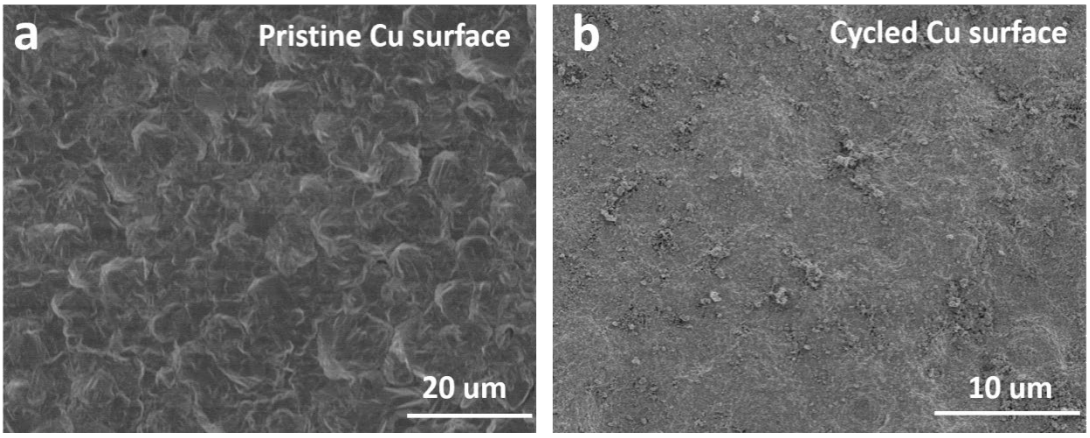

Figure S19. SEM images of pristine Cu-CC (a) and cycled Cu-CC for 80 cycles (b). Before SEM testing, the Cu-CC is cleaned with ethanol several times.

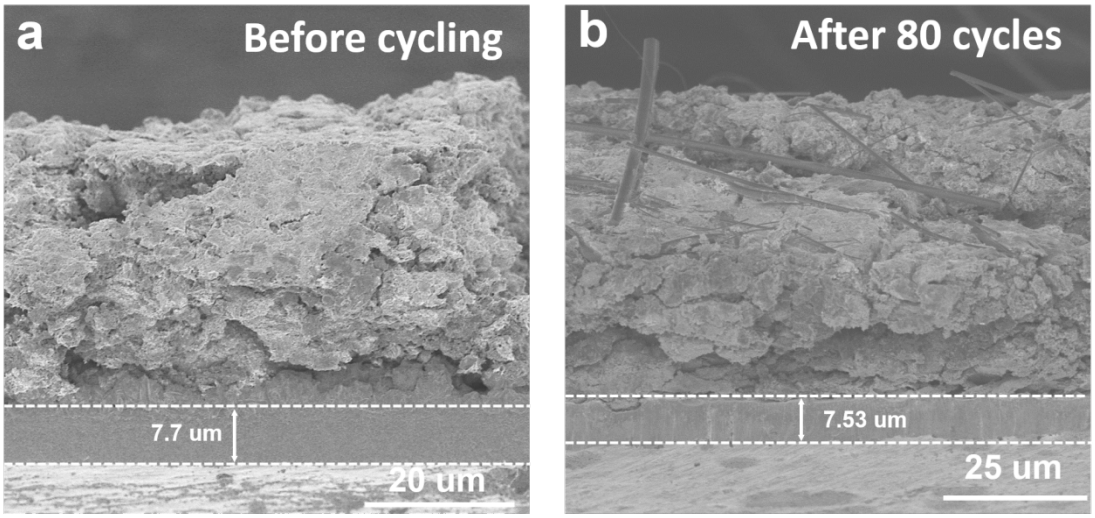

Figure S20. Cross-section SEM images of Cu@CNT/S electrodes with a sulfur loading of 3.5 mg cm^{-2}: (a) pristine electrode, (b) after cycling for 80 cycles.

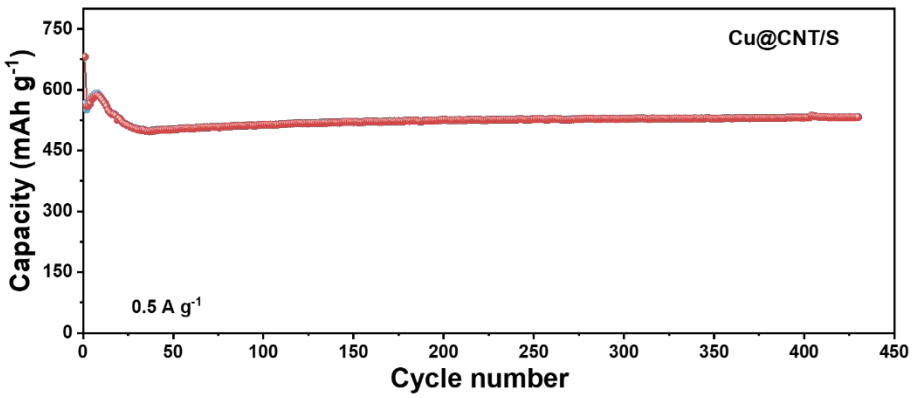

Figure S21. Cycling performance of Cu@CNT/S electrode at 0.5 A g^{-1}.

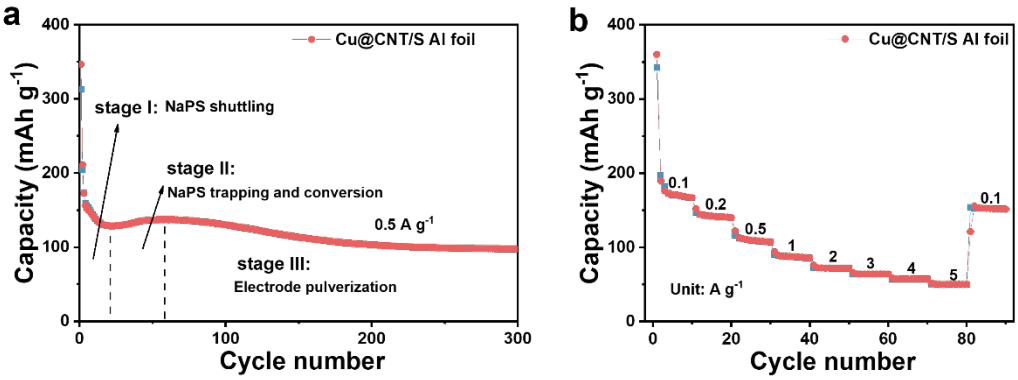

Figure S22. The electricity chemical performance of Cu@CNT/S with Al foil, (a) long cycling performance at 0.5 A g^{-1}, (b) rate performance from 0.1 A g^{-1} to 5 A g^{-1}.

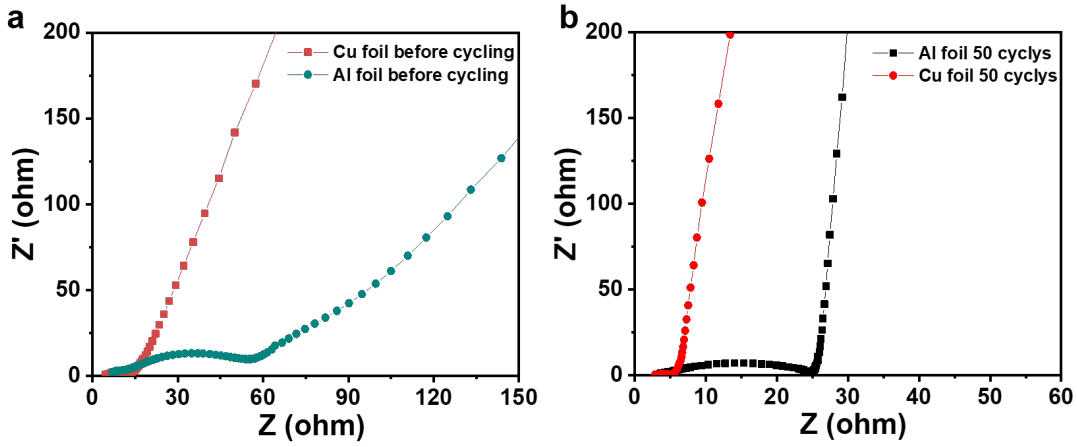

Figure S23. EIS spectra of the Cu@CNT/S electrodes with Cu-CC and Al-CC: (a) before cycling, and (b) after 50 cycles.

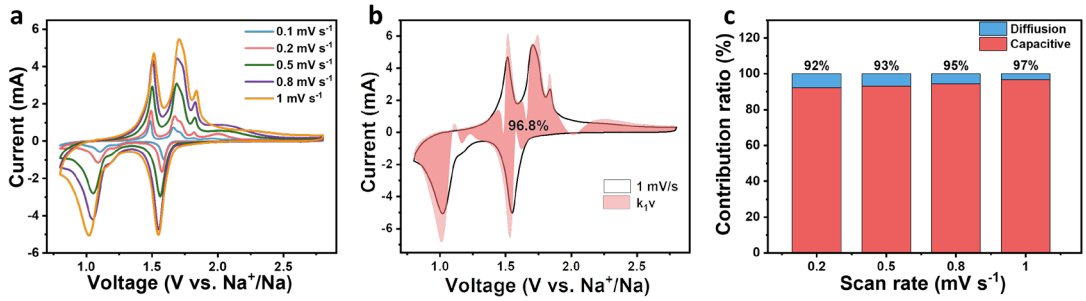

Figure S24. CV curves at various scan rates (a), pseudocapacitive contributions based on scan rates of 1 mV s^{-1} (b), and the different pseudocapacitive contributions based on the cyclic voltammetry (CV) curves at various scan rates (c), in the Cu@CNT/S

electrode.

Table S1. Performance Comparison between our work and published works

Paper	ICE	Cycle life (Cycles)	Capacity retention	Rate	Refs
Adv. Mater. **2021**, *33*, 2103846.	47%	400	~57%	190 mAh g^{-1} at 5 A g^{-1}	[3]
Nat. Commun. **2020**, *11*, 1-11.	~78 %	800	~83%	349 mAh g^{-1} at 5 A g^{-1}	[4]
Nat. Commun. **2021**, *12*, 1-12.	92%	2800	~100%	658.4 mAh g^{-1} at 16.73 A g^{-1}	[5]
Adv. Mater. **2020**, *32*, 1906700.	~35 %	300	~69%	139 mAh g^{-1} at 5 A g^{-1}	[6]
Adv. Mater. **2022**, *34*, 2108363	~59 %	2000	~60%	470 mAh g^{-1} at 5 A g^{-1}	[7]
ACS Nano **2021**, *15*, 15218-15228.	72%	500	~65%	383 mAh g^{-1} at 5 A g^{-1}	[8]
Adv. Funct. Materials **2021**, *31*, 2102280.	~54 %	600	36%	240 mAh g^{-1} at 8.37 A g^{-1}	[9]
Small **2022**, 2106983	~74 %	650	95.8%	759 mAh g^{-1} at 3.35 A g^{-1}	[10]
Adv. Mater. **2022**, *34*, 2204214.	60.2 %	1500	~27%	296 mAh g^{-1} at 10 A g^{-1}	[11]
Adv. Energy Mater. **2020**, *10*, 2000931.	78.6 %	500	90%	304 mAh g^{-1} at 10 A g^{-1}	[12]
J. Mater. Chem. A **2021**, *9*, 3451-3463.	50%	500	~64%	530 mAh g^{-1} at 3.35 A g^{-1}	[13]
Adv. Mater. **2022**, *34*, 2200479.	~70 %	800	~67%	483 mAh g^{-1} at 10 A g^{-1}	[14]
ACS Nano **2022**, *16*, 14178-14187.	~95 %	1000	64%	465 mAh g^{-1} at 5 A g^{-1}	[15]
Adv. Sci. **2020**, *7*,	~63	2000	95%	423 mAh g^{-1} at	[16]

1903246.	%			8.37 A g^{-1}	
Angew. Chem. Int. Edit. **2022**.	~62. 5%	200	65%	486 mAh g^{-1} at 3.35 A g^{-1}	[17]
Nat. Commun. **2021**, *12*, 1-11.	~97. 5%	10000	36%	216 mAh g^{-1} at 3.35 A g^{-1}	[18]
ACS Nano **2021**, *15*, 16207-16217.	~86 %	500	70.28%	550.6 mAh g^{-1} at 8.37 A g^{-1}	[19]
Adv. Sci. **2022**, *9*, 2105544.	~90 %	1000	~64%	461 mAh g^{-1} at 8.37 A g^{-1}	[20]
ACS Nano **2020**, *14*, 7259-7268.	68%	1000	~41%	170 mAh g^{-1} at 5 A g^{-1}	[21]
This work (CNT/S)	88.9 %	1300	98.3%	447.3 mAh g^{-1} at 8 A g^{-1}	
This work (Cu@CNT/S)	83%	1190	~100%	396.9 mAh g^{-1} at 10 A g^{-1}	

REFERENCE

1. Cheng X, Ning R, Li P, Zhang F, Wang K, Jiang J. Structural variations of lignin and lignin-carbohydrate complexes from the fruit shells of Camellia oleifera during ripening. *Int J Biol Macromol* 2023:126946.[DOI:10.1016/j.ijbiomac.2023.126946]

2. Liu H, Gao E, Zhong Z, Wu W, Zhang Z. Clinical application of modified hip joint lateral position in femoral neck fracture. *J Orthop Surg Res* 2023;18:698. [DOI:10.1186/s13018-023-04183-9 PMCID:PMC10506282]

3. Zhang S, Yuan L, Danilova L, et al. Spatial transcriptomics analysis of neoadjuvant cabozantinib and nivolumab in advanced hepatocellular carcinoma identifies independent mechanisms of resistance and recurrence. *Genome Med* 2023;15:72. [DOI:10.1186/s13073-023-01218-y PMCID:PMC10506285]

4. Jamil S, Wang H, Fasehullah M, et al. N doped FeP nanospheres decorated carbon matrix as an efficient electrocatalyst for durable lithium-sulfur batteries. *J Colloid Interface Sci* 2023;630:70-80.[DOI:10.1016/j.jcis.2022.09.126]

5. Hou Q, Wang L, Qi Y, et al. A systematic analysis of the subtilase gene family and expression and subcellular localization investigation of anther-specific members in maize. *Plant Physiol Biochem* 2023;203:108041.[DOI:10.1016/j.plaphy.2023.108041]
6. Yu B, Lin RB, Xu G, et al. Linkage conversions in single-crystalline covalent organic frameworks. *Nat Chem* 2023.[DOI:10.1038/s41557-023-01334-7]
7. Mehar V, Edström H, Shipilin M, et al. Formation of epitaxial PdO(100) during the oxidation of Pd(100). *J Phys Chem Lett* 2023:8493-9.[DOI:10.1021/acs.jpclett.3c01958]
8. Wang L, Ye S, Qin J, Tang M, Dong MY, Fang J. Ferroptosis-related genes LPCAT3 and PGD are potential diagnostic biomarkers for osteoarthritis. *J Orthop Surg Res* 2023;18:699.[DOI:10.1186/s13018-023-04128-2]
9. Jiang W, Yang H. Health spillover studies of long-term care insurance in China: evidence from spousal caregivers from disabled families. *Int J Equity Health* 2023;22:191.[DOI:10.1186/s12939-023-02001-6]
10. Wang C, Zhang M, Liu Y, Cui D, Gao L, Jiang Y. CircRNF10 triggers a positive feedback loop to facilitate progression of glioblastoma via redeploying the ferroptosis defense in GSCs. *J Exp Clin Cancer Res* 2023;42:242.[PMID:37723588 DOI: 10.1186/s13046-023-02816-9]
11. Niu T, Li Z, Huang Y, et al. LFA-1 knockout inhibited the tumor growth and is correlated with treg cells. *Cell Commun Signal* 2023;21:233.[DOI:10.1186/s12964-023-01238-6 PMCID:PMC10506322]
12. Yang M, Su W, Li H, et al. Association of per- and polyfluoroalkyl substances with hepatic steatosis and metabolic dysfunction-associated fatty liver disease among patients with acute coronary syndrome. *Ecotoxicol Environ Saf* 2023;264:115473. [DOI:10.1016/j.ecoenv.2023.115473]
13. Chang CD, Dong C, Zhao SX, et al. Real-world study on the efficacy and safety of first-line antiviral therapy for chronic hepatitis B. *Zhonghua Gan Zang Bing Za Zhi* 2023;31:855-61.[DOI:10.3760/cma.j.cn501113-20230322-00124]

14. Liu B, Zhou X, Yue L, et al. Experts consensus on the procedure of dental operative microscope in endodontics and operative dentistry. *Int J Oral Sci* 2023;15:43. [DOI:10.1038/s41368-023-00247-y]
15. Chen CF, Lucas A, Yin C. Speed limits and locality in many-body quantum dynamics. *Rep Prog Phys* 2023.[PMID:37722374 DOI:10.1088/1361-6633/acfaae]
16. Guo Q, Hu S, Wang S, et al. Comparative analysis of methodologies for predicting overall survival in patients with non-small cell lung cancer based on the number and rate of resected positive lymph nodes: a study based on the SEER database for 2010 through 2019. *Clin Respir J* 2023.[DOI:10.1111/crj.13699]
17. Zhang J, Liu B, Wu J, Wang Z, Li J. DeepCAC: a deep learning approach on DNA transcription factors classification based on multi-head self-attention and concatenate convolutional neural network. *BMC Bioinformatics* 2023;24:345.[DOI:10.1186/s12859-023-05469-9 PMCID:PMC10506269]
18. Ye C, Jing T, Sha Y, Mo M, Yu Z. Two new Trichoderma species (Hypocreales, Hypocreaceae) isolated from decaying tubers of Gastrodiaelate. *MycoKeys* 2023;99:187-207.[PMID:37719304 DOI:10.3897/mycokeys.99.109404 PMCID:PMC10504636]
19. Xiang Y, Mou C, Shi K, et al. SADS-CoV nsp1 inhibits the IFN-β production by preventing TBK1 phosphorylation and inducing CBP degradation. *J Med Virol* 2023;95:e29104.[DOI:10.1002/jmv.29104]
20. Liu Y, Ma S, Rosebrock M, et al. Tungsten nanoparticles accelerate polysulfides conversion: a viable route toward stable room-temperature sodium-sulfur batteries. *Adv Sci* 2022;9:2105544.[PMID:35132807 DOI:10.1002/advs.202105544 PMCID:PMC9008787]
21. Liu H, Pei W, Lai W, et al. Electrocatalyzing S cathodes via multisulfiphilic sites for superior room-temperature sodium-sulfur batteries. *ACS nano* 2020;14:7259-68. [DOI:10.1021/acsnano.0c02488]